First-principles and time-differential γ-γ perturbed-angular-correlation spectroscopy study of structural and electronic properties of Ta-doped TiO_2 semiconductor

G. N. Darriba,[1] L. A. Errico,[1,2] P. D. Eversheim,[3] G. Fabricius,[4] and M. Rentería[1,*]

[1]*Departamento de Física and IFLP (CONICET-UNLP), Facultad de Ciencias Exactas, Universidad Nacional de La Plata, CC 67, 1900 La Plata, Argentina*

[2]*Universidad Nacional del Noroeste Bonaerense (UNNOBA), Monteagudo 2772, 2700 Pergamino, Argentina*

[3]*Helmholtz-Institut für Strahlen- und Kernphysik (ISKP), Universität Bonn, Nussallee 14-16, 53115 Bonn, Germany*

[4]*Instituto de Investigaciones Fisicoquímicas Teóricas y Aplicadas, Facultad de Ciencias Exactas, Universidad Nacional de La Plata, CC 16, 1900 La Plata, Argentina*

(Received 30 December 2008; revised manuscript received 19 February 2009; published 27 March 2009)

The, time-differential γ-γ perturbed-angular-correlation (TDPAC) technique using ion-implanted ^{181}Hf($\rightarrow^{181}$Ta) tracers was applied to study the hyperfine interactions of ^{181}Ta impurities in the rutile structure of TiO_2 single crystals. The experiments were performed in air in the temperature range of 300–1273 K, allowing the electric-field-gradient (EFG) tensor characterization (in magnitude, asymmetry, and orientation) at ^{181}Ta probe atoms located in defect-free cation sites of the structure. The measured EFG is parallel to the [001] crystal axis, as occurs at Ti sites, but normal to the EFG orientation observed at ^{111}Cd impurities in TiO_2 single crystals [L. A. Errico *et al.*, Phys. Rev. Lett. **89**, 055503 (2002)]. In addition, *ab initio* calculations were performed using the full-potential augmented plane wave plus local orbital method that allow us to treat the electronic structure of the doped system and the atomic relaxations induced by the Ta impurity in a fully self-consistent way. We considered different dilutions of the doped system (using the supercell approach) and studied the electronic properties and structural atomic relaxation dependence on the charge state of the impurity. The accuracy of the calculations and the excellent agreement of the predicted magnitude, asymmetry, and orientation of the EFG tensor with the experimental results enable us to infer the EFG sign, not accessible with conventional TDPAC experiments. The comparison of the measured EFG at Ta sites with experimental and *ab initio* theoretical results reported in the literature at Cd, Ta, and Ti sites in TiO_2 allowed us to obtain a deeper insight on the role played by metal impurities in oxide semiconductors.

DOI: 10.1103/PhysRevB.79.115213 PACS number(s): 71.15.−m, 76.80.+y, 61.72.up, 71.55.Ht

I. INTRODUCTION

Hyperfine interaction measurements are widely used experimental techniques that provide local information on the interaction of a probe nucleus with the surrounding electronic charge distribution.[1] In particular, the time-differential γ-γ perturbed-angular-correlation (TDPAC) spectroscopy has been increasingly applied to condensed matter problems through the precise characterization of the electric-field-gradient (EFG) tensor at diluted (ppm) radioactive probe atoms, adequately introduced at substitutional host lattice sites.[1] The characteristics of TDPAC allow detailed investigations of both structural and electronic properties relevant in the fields of solid state physics, chemistry, and biology (see, e.g., Refs. 2–5, and references therein).

In a TDPAC experiment, a suitable probe isotope (generally an impurity in the system under study) is used and the information provided, at this probe site, is given as a product of a nuclear and an extra nuclear quantity. In the case of electric quadrupole interactions, the nuclear quantity is the nuclear-quadrupole moment Q, characteristic of a given nuclear state, which interacts with the EFG at the nuclear position. The information extracted from the experiment is usually expressed by the nuclear-quadrupole frequency ν_Q and the asymmetry parameter η. In this sense, the very well suited (^{111}In$\rightarrow$)^{111}Cd isotope is the most frequently used tracer in TDPAC experiments and has been largely applied to study semiconductor physics, and a large amount of experimental work has been focused on the EFG characterization at ^{111}Cd impurity sites in semiconductor and insulating binary oxides.[6–24]

Due to the fact that the probe atom is an impurity dopant, interpreting experimental EFG results involves the understanding of chemical differences between the probe atom and the indigenous ion replaced by the impurity. All the information that the EFG tensor can provide about the system under study could be obtained by confrontation of the experiment with an accurate prediction of the EFG, such as those obtained with *ab initio* calculations in the framework of the density functional theory (DFT).[25] In this kind of calculation, electronic and structural effects introduced in the host by the presence of the impurity probe (impurity levels, structural distortions, etc.) can be described without the use of arbitrary suppositions. Unfortunately, these calculations prove to be not trivial and time consuming. For this reason, very few EFG calculations have been performed in systems with impurities and the method is far from being routinely applied in this field. In the absence of such predictions at impurity sites, several attempts to correlate experimental results and semiempirical calculations have been made from the very beginning[26,27] in order to describe the different contributions to the EFG at impurity sites.[28] Alternatively, in the case of mainly ionic compounds, the very simple point-charge model (PCM) has been currently used for the interpretation of the experimental EFGs.[20,28] But in this model, charge-transfer effects are only crudely estimated and covalence and the im-

purity character of the probe are completely neglected. Additionally, corrective factors (such as the antishielding Sternheimer's factor γ_∞) must be used in this framework in order to account for the core polarization of the probe atom. Therefore, it is important to study the conditions under which these models and approximations can be used as well as its limitations.

To study the influence of the electronic configuration of the impurity probe atom itself on the EFG it is essential to perform experimental and theoretical studies with different probes in the same crystal structure. In TDPAC experiments, the second most commonly used radioactive probe is ^{181}Hf, which decays by β^- to the ^{181}Ta isotope. In this paper, we present TDPAC experiments in ^{181}Hf($\rightarrow^{181}$Ta)-implanted TiO_2 single crystals and *ab initio* calculations of the EFG at Ta impurities at cation sites in rutile TiO_2. This particular host (TiO_2)-impurity (Ta) combination was suggested by different aspects. Magnitude and symmetry of the EFG tensor have been measured previously by ^{181}Ta TDPAC spectroscopy in polycrystalline TiO_2.[29] Additionally, experimental results for the EFG tensor at Ti nuclei in the rutile structure of pure TiO_2 are known from nuclear magnetic resonance measurements of the ^{49}Ti quadrupole interaction in single crystals.[30] *Ab initio* calculations[31] are in agreement with this experimental result. From the theoretical point of view, different studies were performed in doped rutile TiO_2. In particular, a fully self-consistent *ab initio* determination of the EFG tensor at Cd impurity sites in TiO_2 was reported by some of us.[4] In that work we performed a full-potential linearized-augmented plane wave (FLAPW) calculation of the relaxations introduced by the impurity and studied their interplay with the electronic structure of the system, predicting highly anisotropic relaxations of the nearest neighbors of the impurity and a drastic change in the orientation of the largest principal component, V_{33}, of the EFG tensor with respect to that for Ti atoms in TiO_2. This prediction was confirmed by a key TDPAC experiment[3] and recent *ab initio* calculations.[32] Additionally, the EFG at Ta in TiO_2 has been calculated by Sato *et al.*[33] imposing the constraint of isotropic relaxations of the impurity's nearest oxygen neighbors. In addition to the hypothesis concerning the structural distortions, this calculation has two shortcomings: the size of the supercell (SC) considered in the calculation was very small for a dilute impurity calculation and the charge state of the impurity was not taken into account in a self-consistent way. For these reasons, it looks very interesting to check the validity of this study.

This paper is organized as follows: in Sec. II, details on TDPAC spectroscopy in single crystals and its data analysis are briefly discussed and in Sec. III the experimental EFG results in ^{181}Hf-implanted TiO_2 single crystals are reported. In Sec. IV, the main details of the augmented plane wave (APW)+local orbital (lo) calculations presented in this work are discussed. In Sec. V we present and discuss our theoretical results for the structural relaxations, the electronic structure, and the EFGs for different charge states of the Ta impurity in rutile TiO_2, enlightened by a complete comparison with results obtained with Cd as dopant in the same host. Finally, in Sec. VI we compare our results with those coming from other models and then present our conclusions.

II. EXPERIMENTAL

The TDPAC technique is based on the determination of the influence of extranuclear fields on the correlation between the emission directions of two successive radiations emitted during a nuclear-decay cascade. A complete description of this technique can be found in the literature (see, e.g., Ref. 1). In order to perform the experiments presented in this work we made use of the well known 133–482 keV γ-γ cascade in ^{181}Ta, produced after the β^- nuclear decay of the ^{181}Hf isotope. The experimental perturbation functions, $R(t)$, were analyzed using a multiple-site model for nuclear-electric-quadrupole interaction samples and spin $I=5/2$ of the intermediate level of the γ-γ cascade,[34]

$$R(t) = A_{22}^{\text{expt}}\left(S_{20} + \sum_{n=1}^{3} S_{2n}\cos(\omega_n t)\exp(-\delta\omega_n t)\right), \quad (1)$$

A_{22}^{expt} being the experimental anisotropy of the cascade. The frequencies ω_n are related to the quadrupole frequency $\nu_Q = eQV_{33}/h$ by $\omega_n = g_n(\eta)\nu_Q$. The coefficients g_n are known functions[35] of the asymmetry parameter $\eta=(V_{11}-V_{22})/V_{33}$, where V_{ii} denote the principal components of the EFG tensor, arbitrarily chosen as $V_{33}>V_{22}>V_{11}$. The S_{20} gives a constant contribution to the perturbation function while the S_{2n} $(n=1,2,3)$ are the amplitudes of the contributions with ω_n frequencies.[1] The exponential functions account for a Lorentzian frequency distribution of relative width δ around ω_n. For the nuclear-quadrupole moment of the sensitive intermediate state, $Q=2.36(5)$ b (Ref. 36) is used in this work.

For polycrystalline samples the S_{20} and the S_{2n} coefficients only depend on η. On the other hand, for single crystalline samples these coefficients also depend on the relative orientation of the EFG principal axes with respect to the emission directions $\boldsymbol{k}_1$ and $\boldsymbol{k}_2$ of the two γ rays (which are on the detector plane for detected events), and therefore it exist a particular set of coefficients $S_{Kn}^{\text{eff}}(\boldsymbol{k}_1,\boldsymbol{k}_2,\eta)$ for each crystal orientation. Hence, the TDPAC measurements recorded for a suitable set of crystal orientations enable the determination of the strength, symmetry, and orientation of the EFG tensor.

The TDPAC experiments were performed using the coplanar four BaF_2-detector arrangement at 90° geometry of the PACAr spectrometer (fast-fast logic), which has a high time resolution (0.7 ns) and efficiency for this cascade.[37] A commercially obtained TiO_2 single crystal with the dimensions of $5\times5\times0.5$ mm^3 was used in these experiments. The crystal was cut with the [001] axis perpendicular to the 5×5 mm^2 faces (within 1°) and the [110] axis perpendicular to the 5×0.5 mm^2 sides [results obtained by means of Laue diffraction experiments performed at CECM (Vitry, France)]. The mother isotopes ^{181}Hf of the ^{181}Ta TDPAC probe were implanted at room temperature into the 5×5 mm^2 faces with a energy of 160 keV and a dose of $\approx10^{13}$ ions/cm^2. Following the implantation the single crystal was annealed in air at 800 °C for 6 h in order to remove any radiation damage. After this treatment more than 95% of the probes were found to be located at the regular cation site.

The measurements were carried out at room temperature for two configurations of the sample: "lying sample" ([001] axis normal to the detector plane) and "standing sample" ([001] axis in the detector plane) as a function of "rotation"

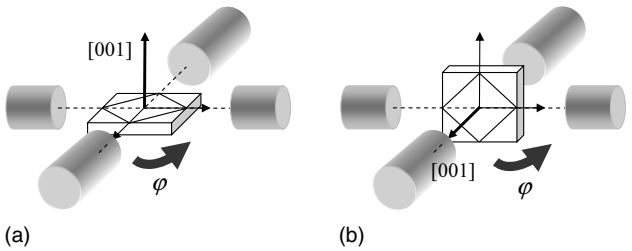

FIG. 1. Single crystal orientations in the present TDPAC experiments. (a) Lying sample ([001] axis normal to the detector plane) and (b) standing sample ([001] axis in the detector plane). φ indicates rotation around an axis normal to detector plane. For the lying sample, $\varphi=0°$ correspond to [110] axis pointing to one detector, while for the standing sample is the [001] axis that points to a detector.

angle φ (see Fig. 1). To determine the S_{2n} $(n=0,1,2,3)$ orientation coefficients, the $R(t)$ spectra were fitted with the perturbation function of Eq. (1), where the S_{2n} coefficients were let free (S_{2n}^{free}) to determine one set of S_{2n}^{free} coefficients for each crystal orientation. The V_{33} orientation with respect to the crystalline axis can be extracted comparing the experimental S_{2n}^{free} and the calculated S_{Kn}^{eff} coefficients,

$$S_{Kn}^{\text{eff}} = \frac{2}{3}[S_{Kn}(180°,\eta) - S_{Kn}(90°,\eta)], \tag{2}$$

where

$$S_{Kn} = \frac{2}{3}\left(S_{22}^{n}(k_1,k_2,\eta) + \frac{A_{42}}{A_{22}}S_{42}^{n}(k_1,k_2,\eta)\right). \tag{3}$$

The S_{22}^{n} and S_{42}^{n} coefficients were calculated according to the formalism presented in Ref. 38.

TDPAC measurements in the temperature range of 300–1273 K where also carried out for the case of the lying sample with $\varphi=45°$. We chose this configuration based on sample stability reasons taking into account the reduced dimensions of the TDPAC furnace, and we chose $\varphi=45°$ because at this angle the $R(t)$ spectra are more suited in order to follow EFG modifications in frequency [see Fig. 2(a)].

III. EXPERIMENTAL RESULTS

Figure 2 shows the $R(t)$ spectra and their corresponding Fourier transforms taken at room temperature for all the series of measurements as a function of the sample orientation. As it was expected, the hyperfine parameters (V_{33}, η, and δ) that characterize each spectra for the 12 orientations in the PAC experiments are similar, being the average values: $V_{33}=14.32(7)$ V/m^2, $\eta=0.555(8)$, and $\delta=0.4(2)\%$. The low distribution observed in the spectra suggests that almost 100% of the probes are located at substitutional cation sites.

As explained in Sec. II, the hyperfine parameters were determined by least-squares fit of Eq. (1) to the experimental data, where the S_{2n} coefficients were let free, and therefore we obtained a set of S_{2n}^{free} coefficients for each different orientation between the sample and the detectors.

For the lying sample configuration ([001] axis perpendicular to the detector plane) the S_{20}^{free} and the S_{21}^{free} coefficients are those that have a strong variation [see Fig. 3(a)]. It can be seen easily in the Fourier spectra [Fig. 2(a)] that S_{20}^{free} diminishes while S_{21}^{free} increases as a function of the rotation angle φ. On the other hand, for the standing sample configuration ([001] axis in the detector plane) the S_{20}^{free} and the S_{22}^{free} coefficients are those that have a strong dependence on φ [Fig. 3(b)]; S_{20}^{free} diminishes again while S_{22}^{free} increases when

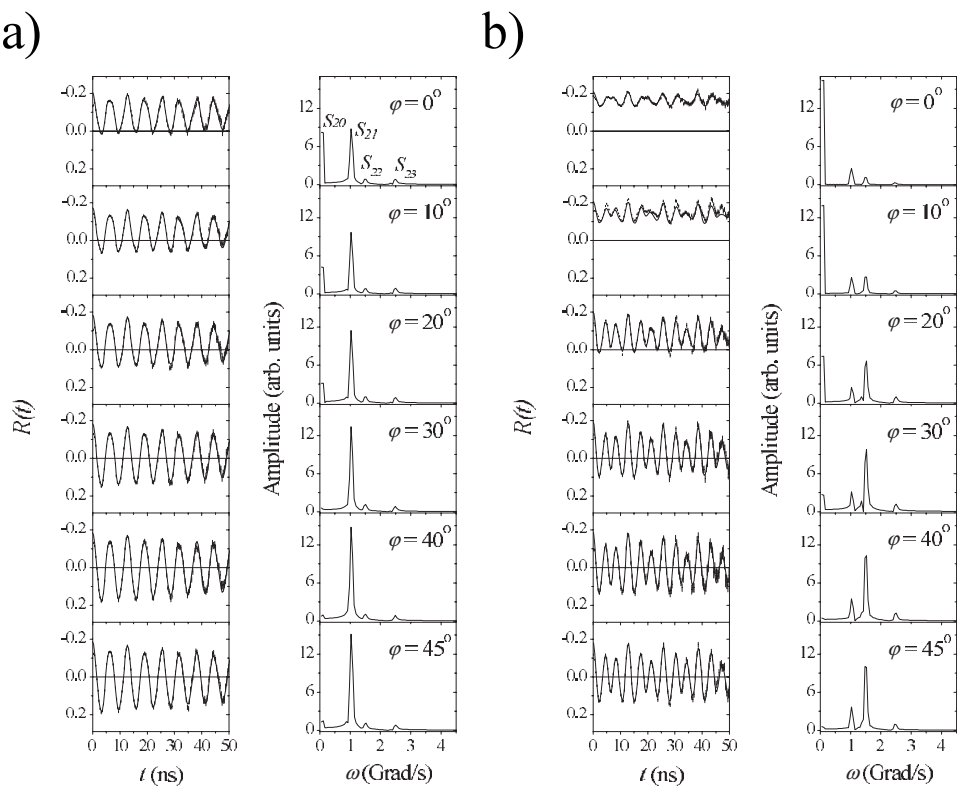

FIG. 2. $R(t)$ spectra (right) and their corresponding Fourier transforms (left) taken at room temperature for (a) lying sample and (b) standing sample.

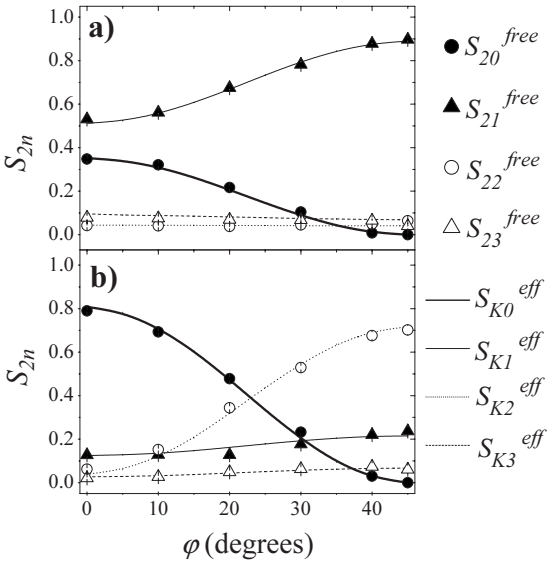

FIG. 3. Comparison between the S_{2n}^{free} coefficients (symbols) and the calculated S_{Kn}^{eff} ones (lines) for $\eta=0.55$ and for (a) V_{33} normal to the detector plane and (b) V_{33} parallel to the detector plane.

the φ rotation angle increases, but this variation is stronger for the standing sample configuration. This behavior of the experimental coefficients suggests that V_{33} is in a direction close to the [001] axis. For this reason, for the S_{Kn}^{eff} calculations of Fig. 3 we assumed an EFG with V_{33} parallel to the [001] crystal axis and, according to the fitted parameters, $\eta=0.55$. Due to the 90° rotation of the oxygen octahedra around neighboring cations [see Figs. 4(a) and 4(b)], the S_{Kn}^{eff} are the average of the coefficients for each of these orientations. In these calculations φ is then the angle between V_{22} and one of the detectors for the lying sample. In the case of the standing sample, φ is the angle between V_{33} and one detector. In Fig. 3 the experimental S_{2n}^{free} and the calculated S_{Kn}^{eff} coefficients are compared. The excellent agreement between experiment and theory clearly determines that V_{33} is parallel to the [001] crystal axis and that V_{22} and V_{11} are both parallel to the [110] crystal axis. The V_{33} orientation is independent of the measuring temperature in the range of 300–1273 K, and the temperature dependence of V_{33} and η is in

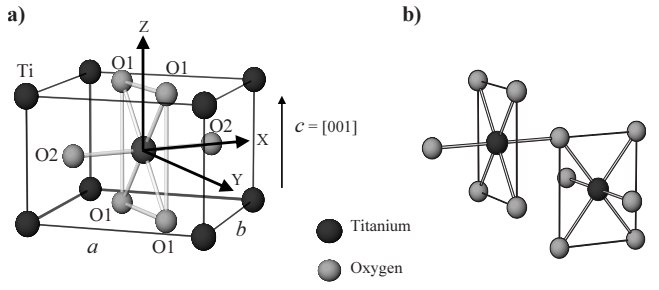

FIG. 4. (a) Rutile TiO_2 structure. All the results discussed in this paper are referred to the axis system indicated here, assuming that the Ta impurity replaces the central Ti atom. (b) Relative orientations presented by the oxygen octahedra around the cation nearest neighbor in the rutile structure, which are rotated one from the other 90° around the c axis.

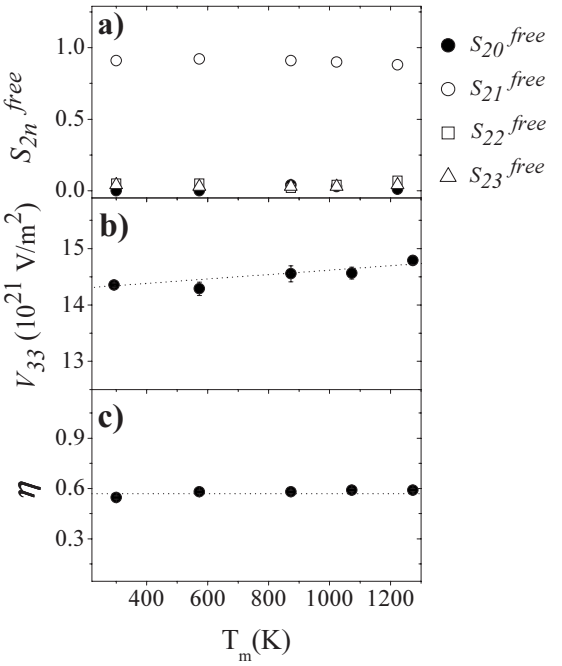

FIG. 5. Evolution of (a) the orientation coefficients S_{2n}^{free} and [(b) and (c)] the fitted hyperfine parameters V_{33} and η, respectively, for ^{181}Hf($\rightarrow^{181}$Ta)-doped TiO_2 single crystal as a function of the measuring temperature T_m. Measurements where carried out for the case of the lying sample with $\varphi=45°$ (see text). Dotted lines represent the experimental results obtained by Adams and Catchen (Ref. 29) in ^{181}Hf($\rightarrow^{181}$Ta)-doped polycrystalline samples of rutile TiO_2.

agreement with that observed in Ref. 29 for ^{181}Ta-doped TiO_2 polycrystalline samples (see Fig. 5).

IV. CALCULATION DETAILS

In order to extract the maximum information from the experiments and to understand the TDPAC results obtained in ^{181}Hf($\rightarrow^{181}$Ta)-doped TiO_2, we performed *ab initio* electronic structure calculations to determine the self-consistent potential and the charge density inside the rutile TiO_2 cell. Our aim here is to obtain from first-principles calculations the hyperfine parameters at a Ta impurity replacing Ti in the host structure, taking properly into account the structural and electronic effects introduced by the impurity in the host lattice. We simulated this nonperiodic system considering a periodically repeated large unit cell where a single Ta atom replaces a single Ti in the rutile TiO_2 host. From these *ab initio* calculations we obtained the equilibrium relaxed structures and the EFG tensor corresponding to a Ta atom at the cation site in the rutile lattice.

In order to simulate an isolated impurity, we employed the supercell method. The SC considered here consists of 12 unit cells of TiO_2 repeated periodically, where one of the 24 Ti atoms is replaced by a Ta atom. This SC gives a composition $Ti_{0.958}Ta_{0.042}O_2$, which represents about 4 at. % of doping. The resulting 72-atom SC (72A-SC) has dimensions $a'=2a=b'=2b=9.17$ Å and $c'=3c=8.86$ Å (Ref. 39) and is also tetragonal with $c/a=0.97$, giving an almost cubic lattice. Each Ta atom is therefore almost equidistant from its Ta

images at a distance of around 9 Å. For checking purposes we have also considered SCs containing 8 and 16 unit cells.

To solve the scalar-relativistic Kohn-Sham equations, theoretical calculations based on the DFT (Ref. 40) have been performed with the APW+lo method,[41] as embodied in the WIEN2K code.[42] In this method the wave functions are expanded in spherical harmonics inside nonoverlapping atomic spheres of radius R_{MT} and in plane waves in the remaining space of the unit cell (the interstitial region). Exchange and correlation effects were treated within DFT using the local density approximation (LDA) (Ref. 43) and the generalized gradient approximation (GGA).[44] We also performed calculations using the recently proposed GGA of Wu and Cohen (WC-GGA),[45] which yields, on average, better results for oxides than the standard GGA. For all the calculations presented in this paper, the atomic spheres radii used for Ta, Ti, and O were 1.10, 0.95, and 0.85 Å, respectively. The parameter RK_{max}, which controls the size of the basis set, was set to 7.0 (R is the smallest muffin-tin radius and K_{max} is the largest wave number of the basis set). Integration in the reciprocal space was performed using the tetrahedron method taking 50 k points in the first Brillouin zone. Once self-consistency of the potential was achieved, quantum-mechanically derived forces were obtained and the ions were displaced according to a Newton-damped scheme, and then the new positions for the atoms were obtained (for details, see Ref. 4). The procedure was repeated until the forces on the ions were below a tolerance value taken as 0.01 eV/Å. At each position, the V_{ii} elements of the EFG tensor were obtained directly from the V_{2M} components of the lattice harmonic expansion of the self-consistent potential.[46]

The precision of the present APW+lo calculations is given by the size of the basis set and the k-mesh sampling. To check the precision of the present results we performed several additional calculations. For selected systems, we increased the basis set (number of plane waves) from $RK_{max}=5$ to $RK_{max}=8$. We also varied the number of k points from 25 to 100. We also studied the effect of the muffin-tin radii on the relevant electronic and structural properties of the system. EFGs and interatomic distances can be obtained with adequate precision using $RK_{max}=7$ and 50 k points (the interatomic distances and the EFG components are converged in less than 0.01 Å and 0.1×10^{21} V/m^2, respectively). Structural relaxation, leading to forces on the atoms of less than 0.01 eV/Å, is the most important factor for convergence of the electronic properties, and they do not change by increasing the number of plane waves or of k points. This is not the same for the total energy that requires a larger number of plane waves and of k points for convergence. But the energy differences are well converged for the employed parameters.

Other sources of error in the present study in order to compare with experiment are the size of the SC considered and the approximations used for the exchange-correlation potential. To check the accuracy of the present study we have performed several additional calculations. In order to check how appropriate are the dimensions of the 72A-SC ($2a\times2a\times3c$) used in the present work we have performed self-consistent electronic structure calculations using a 48A-SC ($2a\times2a\times2c$) and a 96A-SC ($2a\times2a\times4c$). In these calculations we put the nearest oxygen neighbors of Ta at the positions corresponding to the equilibrium in the 72A-SC. We found that the change in the structural relaxations and the EFG is quite small and no significant variations should be expected if larger SCs were considered. The differences between LDA, GGA, and WC-GGA will be discussed in Sec. V. Finally, we note that none of the calculations reported in the present work were spin polarized, but we have checked that no magnetic solution exists at the equilibrium positions.

V. TA-DOPED RUTILE TiO_2: THEORETICAL RESULTS AND DISCUSSION

Before any discussion, an important point must be discussed, which is the charge state of the impurity. Pure TiO_2 is a wide-band-gap semiconductor with the O p band filled and the Ti d band empty. When a Ta^{5+} atom replaces a Ti^{4+} atom, Ta acts as a simple donor impurity. In a previous work we demonstrated that the charge state of the impurity is essential in the description of the structural and electronic properties of the impurity-host system. In effect, different charge states of the impurity can produce different symmetries of the electronic charge distribution in the neighborhood of the impurity and, therefore, different charge states of the impurity can modify the structural relaxations around the impurity and strongly affect the EFG. The question that arises here is as follows: which is the charge state of the impurity that corresponds to the experimental results at 300 K. For this reason, we performed calculations assuming two different physical situations:

(i) We assumed that when a neutral Ta substitutes Ti in rutile TiO_2, it remains in a 5+ valence state. We will name this charge state "neutral charge state" (Ta^0). In this neutral charge state, the impurity level is occupied, and the resulting system is metallic.

(ii) In the real sample, the presence of defects (vacancies, interstitial atoms, and presence of donor or acceptor impurities) or thermal effects can change the charge state of the impurity. In order to investigate this point, we have performed calculations removing one electron from the whole system. We will name this state "charged state" (Ta^+). In this case the impurity donor level is empty.

In the case of the neutral charge state [situation (i)] we used the 72A-SC previously described. To describe situation (ii) we subtracted one electron to the SC that we compensate with a homogeneous negative background in order to have a neutral cell to compute total energy and forces.

A. Structural relaxations

The substitution of a Ti indigenous atom by a Ta impurity produces not negligible forces on its nearest oxygen neighbors (ONN). In order to study the relaxation introduced by the impurity we have considered the Ta and the ONN, displacements until forces vanished [assuming that structural relaxations preserve the point group symmetry of the cell in its initial configuration; this restricts O1 and O2 displacements to yz plane and x axis direction, respectively; see Fig. 4(a)]. We have performed two different relaxation process:

TABLE I. Final distances (in Å) from the Ta (Cd) impurity to its nearest oxygen neighbors for the different calculations performed in Ta (Cd)-doped TiO_2 compared with the ones of the pure oxide.

	TiO_2	
	d(Ti-O1)	*d*(Ti-O2)
Expt.[a]	1.944	1.977
	Ta-doped TiO_2	
	Neutral cell	Charged cell
	d(Ta-O1) *d*(Ta-O2)	*d*(Ta-O1) *d*(Ta-O2)
LDA	1.969 1.985	1.967 1.983
GGA	1.974 1.983	1.974 1.982
WC-GGA	1.973 1.985	1.972 1.984
	Cd-doped TiO_2	
	Neutral cell	Charged cell
	d(Cd-O1) *d*(Cd-O2)	*d*(Cd-O1) *d*(Cd-O2)
LDA[b]	2.153 2.108	2.185 2.111

[a]Reference 39.
[b]References 3 and 4.

(a) allowing the relaxation of the ONN atoms and keeping fixed the other atoms of the supercell; (b) relaxing all atoms in the supercell. We found that the amount of structural relaxation per atom decreases rapidly from the ONN to subsequent shells, leading to minor changes in the positions of the ONN atoms. The EFG at the Ta site is essentially not affected by the relaxation of atoms lying beyond the ONN distance. Due to this fact, none of the conclusions of the present study are affected by the displacement of atoms beyond the ONN distance, thus we will not mention it in what follows.

In Table I we show the equilibrium Ta-ONN distances for the two charge states studied and the different approximations used for the exchange and correlation potential. As can be seen from the results presented in Table I, the ONN relaxes outward, enlarging the Ta-ONN bond lengths. The displacements of each of these O atoms are 0.02 and 0.01 Å for the Ta-O1 and Ta-O2 distances, respectively (1% of the unrelaxed Ta-ONN distances). The relaxed distances are almost independent of the approximations employed for the correlation and exchange potential.

Contrary to the case of the Cd impurity, the results for the relaxations are independent of the impurity charge state. Another important difference between Cd and Ta impurities is that the magnitude of the relaxation introduced by the Ta impurity is very small, while those introduced by Cd are very large and quite anisotropic, with the Cd-O1 distance larger than the Cd-O2 distance, opposite to the initial unrelaxed structure. These different relaxations can be understood by looking at the ionic sizes of the impurities. In effect, we recognize that the Ti^{4+} ion is a member of group IVB, and an estimate of the sixfold coordinated ionic radius is 0.75 Å. The corresponding ionic radius for the Ta^{5+} impurity is 0.78 Å, i.e., very similar to the indigenous Ti ion. On the other hand, the ionic radius of Cd^{2+} is 1.09 A. This simple fact explains the different relaxations introduced by these impurities in the TiO_2 host.

Structural relaxations around impurities were also found in other Ta- and Cd-doped binary oxides: for Cd at both cationic sites in In_2O_3 (Ref. 47) and Lu_2O_3 (Ref. 48) the impurity induced relaxations are around 0.1 Å and larger relaxations, in the range of 0.20–0.25 Å, were found in Cd-doped rutile TiO_2 (Refs. 3 and 4) and SnO_2 (Ref. 49) and in Al_2O_3.[50] All these relaxations can be explained noticing that the bond length of the sixfold coordinated Cd ion in CdO is 2.35 Å, while the bond lengths in In_2O_3, SnO_2, TiO_2, and Al_2O_3 are (in average) 2.20, 2.02, 1.96, and 1.96 Å, respectively. We see that there is a correlation among these movements where the presence of the Cd impurity favors the reconstruction of the bond lengths of Cd in its own oxide, CdO (2.35 Å). Following this idea, the small enlargement of the Ta-ONN bond lengths can be understood from the fact that the bond lengths in tantalum oxide (TaO_2) are about 2.02 Å. As in the case of Cd impurity substitutionally located at cationic sites in binary oxides, it seems that the local structure tries to reconstruct the environment of Ta in its oxide. APW+lo calculations in other binary oxides reported in Refs. 51 and 52 confirm this assertion.

B. Electronic structure and EFGs

We can discuss now the APW+lo predictions for the EFG tensor and compare them with the experimental results. Initially, we calculated the EFG tensor at the unrelaxed positions. As can be seen from the results presented in Table II, all the calculations performed here (LDA, GGA, and WC-GGA) predict the same EFG, so we can conclude (due to the fact that the EFG is very sensitive to small changes in the electronic charge density) that the description of the electronic structure predicted by these calculations is very similar. Another important result is that the EFG is independent

TABLE II. Largest component, V_{33}, of the EFG tensor (in units of 10^{21} V/m^2) and asymmetry parameter η at Ta sites calculated in the unrelaxed structure of rutile TiO_2.

	Neutral cell			Charged cell		
	V_{33}	η	V_{33} direction	V_{33}	η	V_{33} direction
LDA	−16.0	0.03	*Z*	−16.2	0.04	*Z*
GGA	−16.9	0.06	*Z*	−17.1	0.02	*Z*
WC-GGA	−16.6	0.02	*Z*	−16.6	0.00	*Z*

TABLE III. V_{33} (in units of 10^{21} V/m^2), V_{33} direction, and η at the Ta/Cd site (relaxed structures) obtained in the APW+lo calculations compared with experimental TDPAC results at 300 K using $(^{181}\text{Hf}\rightarrow)^{181}\text{Ta}/(^{111}\text{In}\rightarrow)^{111}\text{Cd}$ probes. In order to calculate V_{33} from the experimental nuclear-quadrupole frequencies the following nuclear-quadrupole moments were used: $Q(^{111}\text{Cd})=0.83(14)$ b (Ref. 53); $Q(^{49}\text{Ti})=0.24$ b (Ref. 54); and $Q(^{181}\text{Ta})=2.36(5)$ b (Ref. 36). In all cases, the sign of the experimental V_{33} is unknown.

	TiO_2		
	V_{33}	η	V_{33} direction
Expt.[a]	2.20(1)	0.22(1)	Z
Theor.[b]	−2.09	0.43	Z

	Ta-doped TiO_2					
	Neutral cell			Charged cell		
	V_{33}	η	V_{33} direction	V_{33}	η	V_{33} direction
LDA	−13.0	0.65	Z	−12.5	0.63	Z
GGA	−12.4	0.86	Z	−11.9	0.88	Z
WC-GGA	−12.3	0.83	Z	−12.0	0.80	Z
Expt.	$V_{33}=13.3(1)$	$\eta=0.56(1)$	V_{33} direction$=Z$			

	Cd-doped TiO_2					
	Neutral cell			Charged cell		
	V_{33}	η	V_{33} direction	V_{33}	η	V_{33} direction
LDA[c,d]	−7.16	0.91	X	+4.55	0.26	Y
WC-GGA[e]	+6.0	0.83		+5.00	0.39	
Expt.[c]	$V_{33}=5.34(1)$		$\eta=0.18(1)$		V_{33} direction$=X$ or Y	

[a]Reference 30.
[b]Reference 31.
[c]Reference 3.
[d]Reference 4.
[e]Reference 32.

of the charge state of the impurity. As expected, the main contribution to the EFG at the Ta site comes from the p states (this will be discussed later).

In Table III we present the results for V_{33} and η for the two charge states studied after the structural minimization. It is important to note that, similar to the case of the unrelaxed structure, the resulting EFGs for the two charge states of the impurity are very similar. In the case of LDA, the predicted EFG is in excellent agreement (in magnitude, symmetry, and orientation; see Table III) with the experimental results obtained for the EFG at ^{181}Ta impurities substitutionally located at cationic sites in rutile TiO_2. Moreover, the small differences observed for the EFG for the neutral and the charged charge states of the impurity can be attributed to the very small differences found in the final ONN positions in each case. In order to evaluate the importance of this small changes in the positions of the Ta-ONN on the EFG and to separate electronic and structural effects, we have taken the equilibrium structure of Ta-doped TiO_2 in the neutral charge state obtained using the LDA approximation and performed LDA calculations removing one electron fixing these atomic positions. We obtained that the differences in the V_{ii} components are smaller than 0.05×10^{21} V/m^2 (this difference is inside the convergence error of our calculations). In conclusion, for the same positions of the Ta-ONN, the results for the EFG tensor are absolutely independent of the charge state of the impurity. This result is very different to those obtained for the Cd impurity. In that case, the difference between the EFGs obtained for the charged and neutral cells was very remarkable: the sign, direction, and absolute value of V_{33} were different depending on the charge state of the impurity. We will return to this point soon.

Another important difference between Cd and Ta impurities is the fact that the EFG tensor at Ta sites has the same orientation as the EFG at Ti sites in TiO_2 ([001] in both cases); meanwhile the substitution of a Ti atom by a Cd one produces a change in the EFG tensor orientation. This fact can be explained by the different relaxations that the impurities introduce in the TiO_2 host. In effect, the Cd impurity produces large anisotropic structural relaxations. These relaxations change the local environment around the Cd impurity. The change in the local symmetry around Cd produces a change in the orientation of V_{33} from the [001] to the [110] direction.[3,4] In the case of Ta impurities, the structural distortions introduced by Ta atoms are very small and the final symmetry around Ta is very similar to those of Ti in pure TiO_2. In other words, the magnitude and anisotropy of the structural relaxations induced by the Ta impurity in the TiO_2 host are not enough to change the orientation of the EFG tensor with respect to the pure system. Besides this we have to mention that the small structural relaxations introduced by the Ta impurity play an essential role in the EFG: if we look

at the EFG at Ta site in the unrelaxed structures (see Table II), we obtain an η value that is, in all cases, close to 0.00, in very bad agreement with the experimental results.

In opposite to what has been observed in the case of the unrelaxed structure, the results for the asymmetry parameter η obtained in the LDA calculations are very different from those obtained with GGA and WC-GGA: there is a clear decrease in η going from GGA and WC-GGA to LDA. This apparently discrepancy in the EFG values furnished by the approximations for the exchange and correlation potential used here can be easily understood. In the case of the unrelaxed structure where the calculations were performed with the same atomic positions we have found similar EFGs in all calculations, but, in the case of the relaxed structures, slightly different equilibrium structures were predicted. These results indicate that the different η values obtained in this case can be related to the different equilibrium structures better than to different descriptions of the electronic structure of the doped system. To support this assertion we have performed a series of calculations. (a) We have taken the equilibrium structure predicted by APW+lo-LDA (charged state of the impurity) and, with these positions, we performed an APW+lo-GGA calculation, obtaining in this case $V_{33}=-12.8\times10^{21}$ V/m^2, $\eta=0.68$, the same result obtained in APW+lo using the LDA parametrization ($V_{33}=-13.04\times10^{21}$ V/m^2, $\eta=0.65$); a similar result was found for the neutral charge state. (b) An APW+lo-LDA calculation at the equilibrium positions predicted by APW+lo-GGA, obtaining $V_{33}=-12.3\times10^{21}$ V/m^2, $\eta=0.90$, which is the same result as in the APW+lo-LDA calculation ($V_{33}=-12.4\times10^{21}$ V/m^2, $\eta=0.86$). From these calculations we can conclude that, when we use the same structural positions, LDA, GGA, and WC-GGA predict the same EFG tensor and, as a consequence, the same electronic structure of Ta-doped TiO_2. The differences observed in Table III can then be associated to the different equilibrium structures predicted in each calculation.

We want to understand now the differences between Cd-doped TiO_2 and Ta-doped TiO_2. In particular, we will discuss why the results for the structural relaxations and the EFG tensor are independent of the charge state of the Ta impurity. The EFG tensor is directly related to the anisotropy of the electronic charge density in the vicinity of the nucleus of the probe atom at which the EFG tensor is calculated or measured. The EFG can be decomposed into two contributions:[46] the first one is named the valence contribution since it originates from the nonspherical electron density of the valence (and semicore) electrons within the muffin-tin sphere. This contribution can be further decomposed according to the different orbital symmetries. The second contribution is the lattice contribution originating from more distant regions of the crystal. In most cases (and also in the systems studied here), the valence contribution dominates, while the lattice term is almost negligible. For these reason, in order to investigate the origin of the difference in the EFG for the two mentioned impurities, we concentrate on the valence contribution to the EFG.

When a Cd atom replaces a Ti in the SC, the resulting system is metallic due to the lack of two electrons that are necessary to fill the oxygen p band. Comparison of Figs. 6(a) and 6(b) shows that the presence of Cd in the SC produces the appearance of Cd d levels and impurity states at the top and the bottom of the valence band. The wave function of the impurity state at the Fermi level (E_F) has characters Cd d_{yz}, O1 p_y, and O1 p_z, as shown in Fig. 7(a). Then, providing two electrons to the system implies a drastic change in the symmetry of the electronic charge distribution in the neighborhood of the impurity. This is why we have found different relaxations and EFGs for different charge states of the Cd impurity.

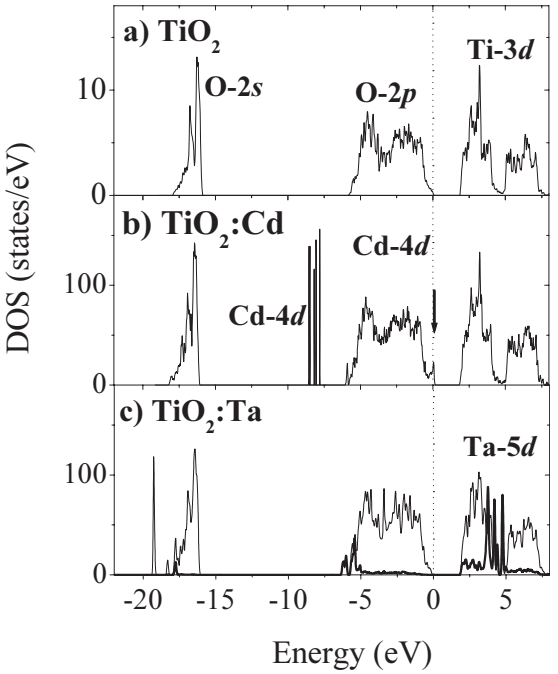

FIG. 6. Total density of states for (a) pure TiO_2, (b) Cd impurities in TiO_2 (neutral cell); the arrow indicates impurity states at the Fermi energy, denoted by a doted vertical line, and (c) Ta impurities in TiO_2 (charged cell). Ta 5d contribution partial density of states (PDOS) is plotted thicker and its amplitude was multiplied by 40 for a better comparison. Energies refer to the Fermi level.

As we said before, Ta in TiO_2 is a simple donor impurity. If we look at the PDOS of the TiO_2:Ta system [see Figs. 6(c) and 7(b)], we can see that the situation is completely different to that of Cd-doped TiO_2. In effect, the Ta5 d levels fall at the same energy as the Ti 3d levels, and impurity levels with a particular symmetry do not appear at the bottom edge of the conduction band. For this reason, removing one electron do not change the symmetry of the charge distribution around Ta and, in consequence, the EFG tensor and the structural relaxations are not affected by changing the charge state of the impurity.

In Table IV we show the total valence contribution to V_{ii} and its components arising from p- and d-orbital symmetries (s-d and higher l contributions are negligible). In the case of the Cd impurity,[4] the largest differences in the EFG between the charged and neutral charge state of the impurity-host system correspond to d components of V_{ii}. This difference originates in the filling of the impurity state at the Fermi level that has an important component of Cd d_{yz}. In the case of Ta, in all cases the Ta p contribution to the EFG is dominant, and

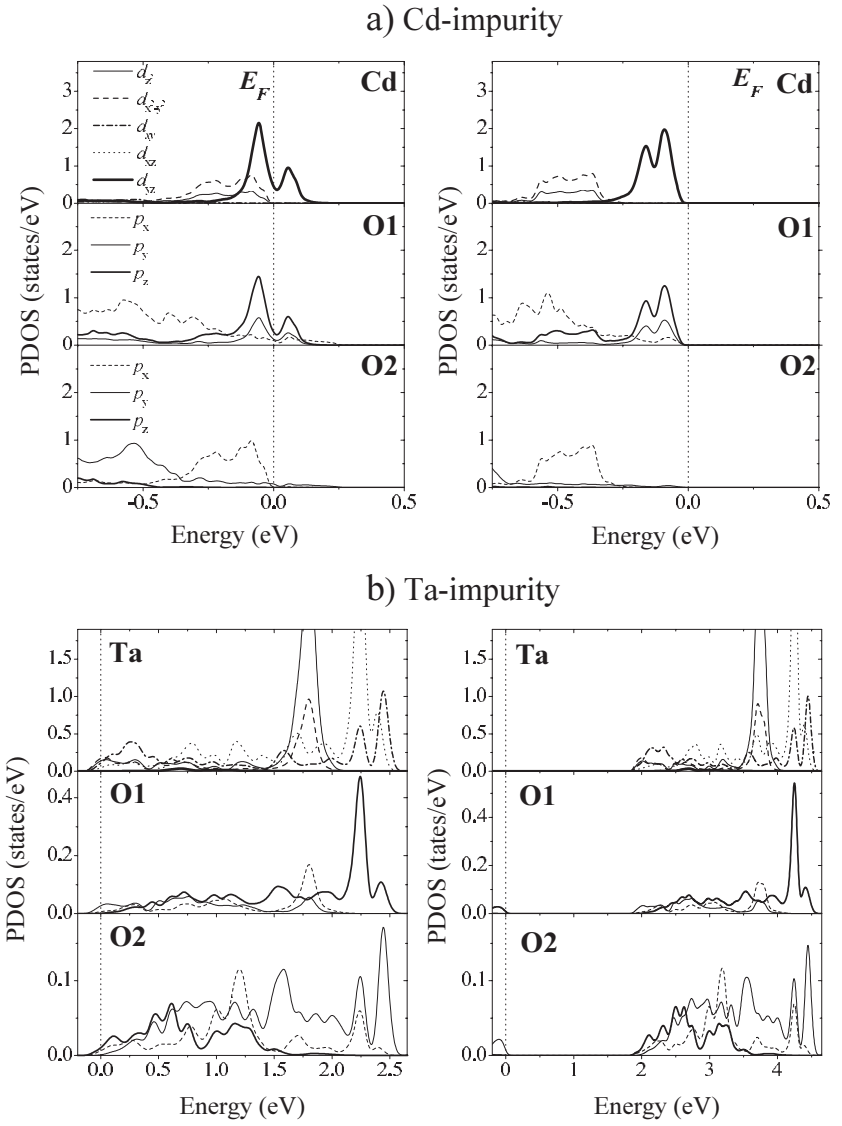

FIG. 7. Atom-resolved PDOS for (a) *d* symmetries of Cd and *p* symmetries of O1 and O2 in TiO_2:Cd and (b) *d* symmetries of Ta and *p* symmetries of O1 and O2 in TiO_2:Ta for the 72A-SC in the neutral state (left) and the charged state (right) of the impurities. Energies are referred to the Fermi level.

the *d* contribution is not altered by the charge state of the impurity. This can be seen in Fig. 7(b), where all the *d* symmetries are present in the impurity state located at the bottom of the conduction band.

C. Temperature dependence of the EFG

The temperature dependence of the EFG at $(^{111}\text{In}\rightarrow)^{111}\text{Cd}$ sites in rutile TiO_2 has been presented in Ref. 29 and explained using *ab initio* calculations in Ref. 55. In this last work, the temperature dependence in the *ab initio* calculations was introduced through the thermal expansion coefficients of the lattice parameters of rutile TiO_2: for each set of lattice parameters the equilibrium position of the Cd-ONN was obtained by force minimization. It was found that the structural relaxations introduced by the Cd impurities change with the lattice parameters or, in other words, with temperature. As we show in Fig. 5, V_{33} at Ta sites in Ta-

TABLE IV. *p*- and *d*-valence contributions to the EFG principal components V_{ii} calculated at Ta sites in rutile TiO_2, in units of 10^{21} V/m^2, for the neutral and charged states in the 72A-SC. Calculations correspond to the LDA approximation.

	Neutral cell			Charged cell		
	V_{11}	V_{22}	V_{33}	V_{11}	V_{22}	V_{33}
p	+2.21	+10.44	−12.65	+2.21	+10.50	−12.71
d	+0.12	+0.77	−0.89	+0.43	+0.61	−1.04
s-d	+0.06	+0.12	−0.18	+0.05	+0.14	−0.19

doped TiO_2 increased linearly with the measuring temperature (T_M); meanwhile the asymmetry parameter is almost independent of T_M. In order to understand the thermal dependence of the EFG at Ta substitutional sites in TiO_2 we follow the same approach employed in the case of the Cd impurity. Our results predicted an increase of about 8% of V_{33} in the range of 300–1273 K and a small decrease in η of about 0.05 in the same temperature range. Both results are in qualitative agreement with the experimental results.

VI. COMPARISON WITH OTHER CALCULATIONS

Different models were proposed in the literature for the EFG at Ta sites in TiO_2. Based in our calculations and the experimental results, we can make a comparative study in order to discard wrong models for the electronic structure and the EFG of Ta-doped rutile TiO_2.

In the case of mainly ionic compounds, the simplest and most widely used approximation for the calculation of the EFG at a probe atom is the point-charge model (PCM).[20] In this approximation the EFG tensor at the probe site is given by $V_{ii}^{\mathrm{PCM}}=(1-\gamma_\infty)V_{ii}^{\mathrm{latt}}$, where V_{ii}^{latt} is the EFG tensor produced by nominal-valence point charges located at the ion positions in the lattice and γ_∞ is the Sternheimer antishielding factor,[20] which depends only on the probe atom amplifying the lattice EFG due to core polarization of the probe atom.

The PCM gives $V_{33}=4.55\times10^{21}$ V/m^2 for TiO_2:Ta, and $\eta=0.40$ pointing along the x direction when a value of -61.24 is used for γ_∞.[56] Our *ab initio* calculations predicted that the Ta impurity induced local distortions in the TiO_2 host. But even if the relaxed coordinates obtained in our *ab initio* calculations were used, the PCM would fail in the description of the EFG, giving $V_{33}=-5.66\times10^{21}$ V/m^2 and $\eta=0.30$ (x direction), in clear contradiction with $V_{33}=-13.0\times10^{21}$ V/m^2 and $\eta=0.65$ (z direction) that we obtain from the self-consistent APW+lo calculation, results that were confirmed by the TDPAC results. From this discussion it is clear that the failure of the PCM prediction of the EFG at impurity sites is not only due to the use of wrong atomic positions but to a wrong description of the electronic structure of the impurity-host system, in particular in the subnanoscopic neighborhood of the impurity.

In a previous work Sato *et al.*[33] performed self-consistent electronic structure calculations in Ta-doped TiO_2 with a 12-atom SC (dimensions: $a'=a$, $b'=b$, and $c'=2c$), but they assumed that the relaxations of the nearest oxygen neighbors of the Ta atom were isotropic. Additionally, relaxations were performed only for the neutral charge state of the impurity, and at the end of the relaxation process one electron was remove to compute the EFG without computing the self-consistent potential of the charged cell. They obtained d(Ta-O1)=2.08 Å, d(Cd-O2)=2.12 Å (enlargement of 7% of the unrelaxed Ta-ONN bond lengths). The result for the EFG tensor was $V_{33}=-11.76\times10^{21}$ V/m^2 and $\eta=0.34$, pointing along the z direction. It is interesting to note that these results also agree with the available experimental information. We understand that this agreement is fortuitous due to the reduced SC used, the isotropic relaxation assumed, and the rigid-band model used to change the charge state of the impurity.

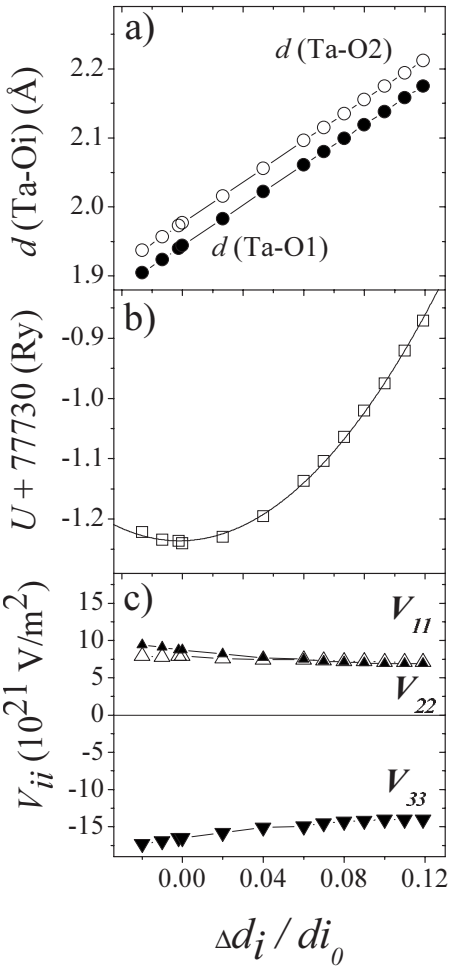

FIG. 8. Isotropic relaxation process of the Ta-ONN distances for the case of the charged cell (similar results were obtained for the neutral case). Distances $d_1=d$(Ta-O1) and $d_2=d$(Ta-O2), total energy, and EFG principal components (V_{ii}) are shown as a function of the relative displacement, $\Delta di/di_0$, of the nearest oxygen atoms ($\Delta d_i=d_i-di_0$, di_0 is d_i for the pure system).

A question that arises at this point is if self-consistent electronic APW+lo calculations performed with a converged SC give an EFG compatible with the experimental results or not when relaxations of the oxygen NN of the Ta atom are constrained to be isotropic. We have performed self-consistent calculations for the 72A-SC (in the case of the charged cell) for different positions of O1 and O2 atoms but moving them inward and outward along the bond lengths, keeping the relation d(Ta-O1)/d(Ta-O2) constant. We obtained that the Ta-ONN distances that minimize the energy of the system [see Fig. 8(a)] are 1.94 and 1.97 Å for O1 and O2 atoms, respectively, i.e., a contraction of 0.2% of the unrelaxed distances. At the equilibrium position we obtained for V_{33} a value of -16.5×10^{21} V/m^2 (pointing in the [001] direction) and an η value of 0.04, in bad agreement with the experimental results, confirming that an isotropic relaxation is not consistent with the experimental data. Moreover, the free relaxation process gives an equilibrium structure with an

energy of 1.5 eV smaller than those corresponding to the isotropic relaxations.

To conclude, we want to mention that in a recent publication, Ryu *et al.*[32] presented a theoretical and TDPAC study of the EFG tensor at ^{44}Sc impurity sites in the rutile and anatase phases of TiO_2. The authors reported an almost antiaxial EFG with $\eta=0.94(1)$ and $V_{33}=2.02(19)\times10^{21}$ V/m^2. *Ab initio* calculations, performed using the same code and methodology than those described in the present work, predict that the distances Sc-O1 and Sc-O2 are enlarged from 1.94 and 1.98 to 2.068 and 2.055 Å. Since the average Sc-ONN bond lengths in its oxide (Sc_2O_3) are 2.14 Å, the reported structural distortions are in agreement with our picture that the local structure tries to reconstruct the environment of the impurities in its oxide. The *ab initio* APW+lo calculations predict $\eta=0.75$ and $V_{33}=+2.04\times10^{21}$ V/m^2, in very good agreement with the experiments.

VII. CONCLUSIONS

In this work we present an experimental TDPAC and *ab initio* APW+lo theoretical study of structural and electronic properties of the ^{181}Hf($\rightarrow^{181}$Ta)-doped rutile TiO_2 semiconductor. The combination of the experiments and the calculations enabled the complete EFG characterization at Ta sites located at defect-free cation sites, predicting a negative EFG sign with high accuracy.

The experimental EFG orientation resulted parallel to the [001] crystal axis, as in the case of Ti sites in pure TiO_2, but perpendicular to the EFG measured at Cd-doped TiO_2. Their comparison with the APW+lo predictions shows that strong anisotropic relaxations of the nearest oxygen neighbors of the Cd atoms produce this change in the EFG orientation.

The structural atomic relaxations (expansions) introduced by the Ta impurity are rather small, independent of its charge state and of the exchange-correlation approximation used, and the EFG is mainly affected by the Ta ONN relaxations. This behavior is opposite to that presented by Cd, but this can be understood by the different ionic radii of the impurities and the impurity-ONN mean bond length in their respective oxides, CdO and TaO_2, scenario ruled out from other binary oxide studies.

We showed that the different exchange-correlation approximations make a similar description of the electronic structure in the TiO_2:Ta system and that the slight changes in the EFG are only due to the small differences in the equilibrium positions for each approximation. The small expansion of the Ta-ONN bond lengths predicted in any of the approximations cannot change the orientation of the EFG. However, the slightly different structural distortions predicted by GGA and WC-GGA with respect to LDA influence the final value of the asymmetry parameter.

The presence of the Ta impurities in the TiO_2 semiconductor introduces impurity states both in the valence and the conduction bands, but there is not a relevant impurity level that shows a certain orbital symmetry near the Fermi energy, as was the case for Cd in TiO_2. In effect, Ta introduces donor impurity states in the conduction band but they are rather flat and all the *d* symmetries are present on them. The removal of one electron from this donor states does not produce a change in the 5*d* EFG contribution, thus leaving the EFG (originated mainly in the 6*p* contribution) unaltered. Unfortunately, due to this behavior, we cannot determine unambiguously the charge state of the impurity in this impurity-host system.

Finally, we showed that a simple model for the EFG, such as the PCM, with or without relaxing the host atoms, does not reproduce the EFG orientation and magnitude. Even more, PCM fails in the prediction of the orientation of the EFG at Ti sites in pure TiO_2. This discrepancy cannot be attributed to structural distortions. The discrepancy between the PCM and the results obtained at Cd, Ta, and Ti atoms in rutile TiO_2 is originated in the symmetry of the dominant valence contribution to the EFG, the *p* symmetry in these cases. In the same sense, simple assumptions such as isotropic relaxations around the Ta impurity give a wrong value for the asymmetry parameter and a system energy higher than that of the free relaxation process.

ACKNOWLEDGMENTS

This work was partially supported by Agencia Nacional de Promoción Científica y Tecnológica (ANPCyT) (PICT98 03-03727), Consejo Nacional de Investigaciones Científicas y Técnicas (CONICET) (PIP6032), Fund. Antorchas, Argentina, and Third World Academy of Sciences (TWAS), Italy (RGA 97-057). The neutron irradiation performed by the GKSS reactor FRG-1, Germany, is kindly acknowledged. This research made use of the HP-Parallel-Computing Bose Cluster and the computational facilities of the Physics of Impurities (PhI) group at IFLP and Departamento de Física (UNLP). M.R. is indebted to J-P. Dallas (CECM, Vitry) for the single crystals orientation and to A. Traverse (LCP, Orsay, France) for valuable support on this project.

*Corresponding author; renteria@fisica.unlp.edu.ar

[1] See, e.g., G. Schatz and A. Weidinger, *Nuclear Condensed Matter Physics: Nuclear Methods and Applications* (Wiley, Chichester, 1996); E. N. Kaufmann and R. J. Vianden, Rev. Mod. Phys. **51**, 161 (1979); H. Frauenfelder and R. M. Steffen, in *Alpha-, Beta-, and Gamma-Ray Spectroscopy*, edited by K. Siegbahn (North-Holland, Amsterdam, 1966), Vol. 2.

[2] A. Lerf and T. Butz, Angew. Chem., Int. Ed. Engl. **26**, 110 (1987); T. Klas, J. Voigt, W. Keppner, R. Wesche, and G. Schatz, Phys. Rev. Lett. **57**, 1068 (1986); R. Vianden and U. Feuser, *ibid.* **61**, 1981 (1988); N. Achtziger and W. Witthuhn, Phys. Rev. B **47**, 6990 (1993); D. Lupascu, M. Uhrmacher, and K. P. Lieb, J. Phys.: Condens. Matter **6**, 10445 (1994); S. Lany, P. Blaha, J. Hamann, V. Ostheimer, H. Wolf, and T. Wichert, Phys. Rev. B **62**, R2259 (2000); J. Meersschaut, C. L'abbe, M. Rots, and S. D. Bader, Phys. Rev. Lett. **87**, 107201 (2001); J. M. Ramallo-López, M. Rentería, E. E. Miró, F. G. Requejo, and A. Traverse, *ibid.* **91**, 108304 (2003); M. Forker, S. Muller, P. de la

Presa, and A. F. Pasquevich, Phys. Rev. B **68**, 014409 (2003).
[3] L. A. Errico, G. Fabricius, M. Rentería, P. de la Presa, and M. Forker, Phys. Rev. Lett. **89**, 055503 (2002).
[4] L. A. Errico, G. Fabricius, and M. Rentería, Phys. Rev. B **67**, 144104 (2003).
[5] L. A. Terrazos, H. M. Petrilli, M. Marszalek, H. Saitovich, P. R. J. Silva, P. Blaha, and K. Schwarz, Solid State Commun. **121**, 525 (2002).
[6] L. A. Errico, M. Rentería, A. G. Bibiloni, and F. G. Requejo, Hyperfine Interact. **120-121**, 457 (1999).
[7] A. G. Bibiloni, J. Desimoni, C. P. Massolo, L. Mendoza-Zélis, A. F. Pasquevich, F. H. Sánchez, and A. López-García, Phys. Rev. B **29**, 1109 (1984).
[8] H. Wolf, S. Deubler, D. Forkel-Wirth, H. Foettinger, M. Iwatschenko-Borho, F. Meyer, M. Renn, W. Witthuhn, and R. Helbig, Mater. Sci. Forum **10-12**, 863 (1986).
[9] W. Bolse, M. Uhrmacher, and K. P. Lieb, Phys. Rev. B **36**, 1818 (1987).
[10] C. P. Massolo, M. Rentería, J. Desimoni, and A. G. Bibiloni, Phys. Rev. B **37**, 4743 (1988).
[11] A. G. Bibiloni, J. Desimoni, C. P. Massolo, and M. Rentería, Phys. Rev. B **38**, 20 (1988).
[12] F. G. Requejo, A. G. Bibiloni, C. P. Massolo, J. Desimoni, and M. Rentería, Phys. Status Solidi A **116**, 503 (1989).
[13] M. S. Moreno, A. G. Bibiloni, C. P. Massolo, J. Desimoni, and M. Rentería, Phys. Rev. B **40**, 2546 (1989).
[14] J. Desimoni, A. G. Bibiloni, C. P. Massolo, and M. Rentería, Phys. Rev. B **41**, 1443 (1990).
[15] A. F. Pasquevich, M. Uhrmacher, L. Ziegeler, and K. P. Lieb, Phys. Rev. B **48**, 10052 (1993).
[16] M. Rentería, D. Wiarda, A. G. Bibiloni, and K. P. Lieb, Hyperfine Interact. **60**, 679 (1990).
[17] M. Rentería, A. G. Bibiloni, M. S. Moreno, J. Desimoni, R. C. Mercader, A. Bartos, M. Uhrmacher, and K. P. Lieb, J. Phys.: Condens. Matter **3**, 3625 (1991).
[18] J. Shitu, M. Rentería, C. P. Massolo, A. G. Bibiloni, and J. Desimoni, Int. J. Mod. Phys. B **6**, 2345 (1992).
[19] Th. Wenzel, A. Bartos, K. P. Lieb, M. Uhrmacher, and D. Wiarda, Ann. Phys. **504**, 155 (1992).
[20] D. Wiarda, M. Uhrmacher, A. Bartos, and K. P. Lieb, J. Phys.: Condens. Matter **5**, 4111 (1993).
[21] D. Lupascu, J. Albohn, J. Shitu, A. Bartos, K. Królas, M. Uhrmacher, and K. P. Lieb, Hyperfine Interact. **80**, 959 (1993).
[22] M. Neubauer, A. Bartos, K. P. Lieb, D. Lupascu, M. Uhrmacher, and Th. Wenzel, Europhys. Lett. **29**, 175 (1995).
[23] D. Lupascu, S. Habenicht, K. P. Lieb, M. Neubauer, M. Uhrmacher, and Th. Wenzel, Phys. Rev. B **54**, 871 (1996).
[24] J. Luthin, K. P. Lieb, M. Neubauer, M. Uhrmacher, and B. Lindgren, Phys. Rev. B **57**, 15272 (1998).
[25] H. Akai, M. Akai, S. Blügel, B. Drittler, H. Ebert, K. Terakura, R. Zeller, and P. H. Dederiches, Prog. Theor. Phys. **101**, 11 (1990).
[26] W. Bolse, A. Bartos, J. Kesten, M. Uhrmacher, and K. P. Lieb, in *XXIII Zacopane School on Physics*, edited by K. Królas and K. Tomala (Institute of Nuclear Physics, Cracow, 1988).
[27] J. Kesten, W. Bolse, K. P. Lieb, and M. Uhrmacher, Hyperfine Interact. **60**, 683 (1990).
[28] M. Rentería, C. P. Massolo, and A. G. Bibiloni, Mod. Phys. Lett. B **6**, 1819 (1992).
[29] J. M. Adams and G. L. Catchen, Phys. Rev. B **50**, 1264 (1994).
[30] O. Kanert and H. Kolem, J. Phys. C **21**, 3909 (1988).
[31] P. Blaha, D. J. Singh, P. I. Sorantin, and K. Schwarz, Phys. Rev. B **46**, 1321 (1992).
[32] S. B. Ryu, S. K. Das, T. Butz, W. Schmitz, Ch. Spiel, P. Blaha, and K. Schwarz, Phys. Rev. B **77**, 094124 (2008).
[33] K. Sato, H. Akai, and T. Minamisono, Z. Naturforsch., A: Phys. Sci., **53**, 396 (1998).
[34] M. Rentería, F. G. Requejo, A. G. Bibiloni, A. F. Pasquevich, J. Shitu, and K. Freitag, Phys. Rev. B **55**, 14200 (1997).
[35] L. A. Mendoza-Zélis, A. G. Bibiloni, M. C. Caracoche, A. R. López-García, J. A. Martínez, R. C. Mercader, and A. F. Pasquevich, Hyperfine Interact. **3**, 315 (1977).
[36] T. Butz and A. Lerf, Phys. Lett. **97A**, 217 (1983).
[37] M. Rentería, A. G. Bibiloni, G. N. Darriba, L. A. Errico, E. L. Muñoz, D. Richard, and J. Runco, Hyperfine Interact. **181**, 145 (2008).
[38] D. Wegner, Hyperfine Interact. **23**, 179 (1985).
[39] R. J. Hill and C. J. Howard, J. Appl. Crystallogr. **20**, 467 (1987).
[40] P. Hohenberg and W. Kohn, Phys. Rev. **136**, B864 (1964); W. Kohn and L. J. Sham, *ibid.* **140**, A1133 (1965).
[41] E. Sjöstedt, L. Nordström, and D. J. Singh, Solid State Commun. **114**, 15 (2000); G. K. H. Madsen, P. Blaha, K. Schwarz, E. Sjöstedt, and L. Nordström, Phys. Rev. B **64**, 195134 (2001); see also S. Cottenier, *Density Functional Theory and the Family of (L)APW-Methods: A Step-by-Step Introduction* (KU Leuven, Belgium, 2002) (http://www.wien2k.at/reg_user/textbooks).
[42] P. Blaha, K. Schwarz, G. Madsen, D. Kvasnicka, and J. Luitz, *WIEN2k, An Augmented Plane Wave Plus Local Orbitals Program for Calculating Crystal Properties* (Karlheinz Schwarz, Technical Universität Wien, Austria, 1999).
[43] J. P. Perdew and Y. Wang, Phys. Rev. B **45**, 13244 (1992).
[44] J. P. Perdew, K. Burke, and M. Ernzerhof, Phys. Rev. Lett. **77**, 3865 (1996).
[45] Z. Wu and R. E. Cohen, Phys. Rev. B **73**, 235116 (2006).
[46] P. Blaha, K. Schwarz, and P. H. Dederichs, Phys. Rev. B **37**, 2792 (1988); K. Schwarz, C. Ambrosch-Draxl, and P. Blaha, *ibid.* **42**, 2051 (1990).
[47] L. A. Errico, M. Rentería, G. Fabricius, and G. N. Darriba, Hyperfine Interact. **158**, 63 (2004).
[48] L. A. Errico, M. Rentería, A. G. Bibiloni, and G. N. Darriba, Phys. Status Solidi C **2**, 3576 (2005).
[49] L. A. Errico, G. Fabricius, and M. Rentería, Hyperfine Interact. **136-137**, 749 (2001).
[50] M. Rentería, G. N. Darriba, L. A. Errico, E. L. Muñoz, and P. D. Eversheim, Phys. Status Solidi B **242**, 1928 (2005).
[51] L. A. Errico, G. Fabricius, and M. Rentería, Phys. Status Solidi B **241**, 2394 (2004).
[52] R. E. Alonso, L. A. Errico, E. L. Peltzer y Blancá, A. López-García, A. Svane, and N. E. Christensen, Phys. Rev. B **78**, 165206 (2008).
[53] P. Herzog, K. Freitag, M. Reuschenbach, and H. Walitzki, Z. Phys. A **294**, 13 (1980).
[54] R. Vianden, Hyperfine Interact. **16**, 1081 (1983).
[55] L. A. Errico, Hyperfine Interact. **158**, 29 (2004).
[56] F. D. Feiock and W. R. Johnson, Phys. Rev. **187**, 39 (1969). In the case of Ta^{5+}, the value came from interpolation between the Hf^{4+} and W^{6+} values.